Design and Synthesis of Conformationally Constrained Grb2 SH2 Domain Binding Peptides Employing α-Methylphenylalanyl Based Phosphotyrosyl Mimetics

Shinya Oishi,[†] Rajeshri G. Karki,[†] Sang-Uk Kang,[†] Xiangzhu Wang,[†] Karen M. Worthy,[‡] Lakshman K. Bindu,[‡] Marc C. Nicklaus,[†] Robert J. Fisher,[‡] and Terrence R. Burke Jr.*[,†]

Laboratory of Medicinal Chemistry, Center for Cancer Research, National Cancer Institute, National Institutes of Health, Frederick, Maryland 21702, and Protein Chemistry Laboratory, Science Applications International Corporation−Frederick, Frederick, Maryland 21702

Received September 7, 2004

Previous work has shown that incorporation of either 1-aminocyclohexanecarboxylic acid (Ac_6c) or α-methyl-*p*-phosphonophenylalanine ((α-Me)Ppp) in the phosphotyrosyl (pTyr) C-proximal position (pY + 1 residue) of Grb2 SH2 domain binding peptides confers high affinity. The tetralin-based (*S*)-2-amino-6-phosphonotetralin-2-carboxylic acid (Atc(6-PO_3H_2)) simultaneously presents structural features of both (α-Me)Ppp and Ac_6c residues. The current study compares the affinity of this tetralin hybrid Atc(6-PO_3H_2) versus Ac_6c and (α-Me)Ppp residues when incorporated into the pY + 1 position of a high-affinity Grb2 SH2 domain binding tripeptide platform. The highest binding affinity (K_D = 14.8 nM) was exhibited by the (α-Me)Ppp-containing parent, with the corresponding Ac_6c-containing peptide being nearly 2-fold less potent (K_D = 23.8 nM). The lower K_D value was attributable primarily to a 50% increase in off-rate. Replacement of the Ac_6c residue with the tetralin-based hybrid resulted in a further 4-fold decrease in binding affnity (K_D = 97.8 nM), which was the result of a further 6-fold increase in off-rate, offset by an approximate 45% increase in on-rate. Therefore, by incorporation of the key structural components found in (α-Me)Ppp into the Ac_6c residue, the tetralin hybrid does enhance binding on-rate. However, net binding affinity is decreased due to an associated increase in binding off-rate. Alternatively, global conformational constraint of an (α-Me)Ppp-containing peptide by β-macrocyclization did result in pronounced elevation of binding affinity, which was achieved primarily through a decrease in the binding off-rate. Mathematical fitting using a simple model that assumed a single binding site yielded an effective K_D of 2.28 nM. However this did not closely approximate the data obtained. Rather, use of a complex model that assumed two binding sites resulted in a very close fit of data and provided K_D values of 97 pM and 72 nM for the separate sites, respectively. Therefore, although local conformational constraint in the pY + 1 residue proved to be deleterious, global conformational constraint through β-macrocyclization achieved higher affinity. Similar β-macrocyclization may potentially be extended to SH2 domain systems other than Grb2, where bend geometries are required.

The growth factor receptor bound protein 2 (Grb2) is an SH2 domain containing noncatalytic module that provides important connectivity in protein tyrosine kinase (PTK)-dependent signaling associated with a variety of cancers.[1−6] Accordingly, significant effort has been expended in developing Grb2 SH2 domain binding antagonists as potential therapeutics.[7−9] On the basis of the preferred binding of Grb2 SH2 domains to phosphotyrosyl (pTyr)-containing sites of the sequence "pY-X-N", tripeptide **1** (Figure 1) was identified by Novartis scientists as a high-affinity ligand that is characterized by a (pY + 1)-positioned[10] 1-aminocyclohexanecarboxylic acid residue (Ac_6c) (side chain shown as **2**, Figure 1).[11] The Ac_6c residue had been shown to be optimal for the pY + 1 position due to its ability to induce the β-bend conformation needed for binding and to provide good van der Waals interactions with Phe βD5 (F108) and Gln βD3 (Q106) residues.[12] More recently, a significant discovery related to the pY + 1 residue was reported by Garbay et al., who, using a different peptide platform, showed that insertion of an (α-methyl)pTyr residue (side chain shown as **3**, Figure 1)[13] or a pTyr mimetic such as α-methyl-*p*-phosphonophenylalanine ((α-Me)Ppp) (side chain shown as **4**, Figure 1)[14] enhances the Grb2 SH2 domain binding affinity of short peptide sequences through ionic interactions of the negatively charged phosphate mimetic with the positively charged guanidino group of the Arg BG4 (R142) residue.[15] To date, Ac_6c and (α-Me)Ppp are among the highest affinity pY + 1 residues identified for Grb2 SH2 domain binding peptides. An unrelated advance in Grb2 SH2 domain binding inhibitor design is the induction of global conformational constraint through macrocyclization originating at the pTyr mimetic β-position.[16,17] Significant affinity enhancements have been achieved in going from open chain analogues such as **6** to macrocyclic variants such as **7**.[18−21]

* Author to whom correspondence should be addressed. Address: CCR, NCI; NIH; P.O. Box B, Bldg. 376 Boyles St.; Frederick, MD 21702-1201. Phone: (301) 846-5906. Fax: (301) 846-6033. E-mail: tburke@helix.nih.gov.
[†] CCR, NCI, NIH.
[‡] SAIC−Frederick.

10.1021/jm0492709 CCC: $30.25
Published on Web 01/19/2005

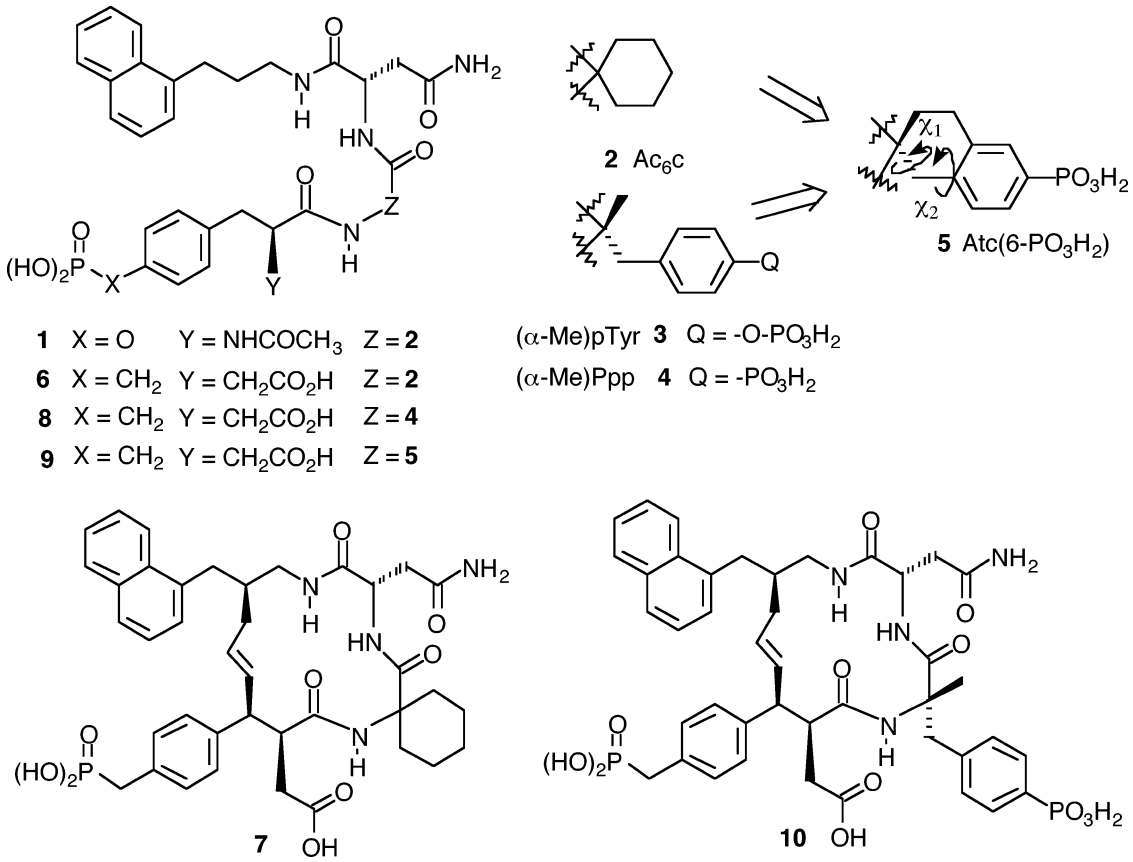

Figure 1. Structures of analogues discussed.

The affinity-enhancing effects of Ac_6c residues and β-macrocyclization are in principle due to conformational restrictions leading to induction of β-bend geometries, whereas the binding effects of pY + 1 (α-Me)pTyr mimetics can be attributed predominately to ionic interactions. Because these two modalities differ mechanistically, the question arose as to what effects could result from combining together features found individually in (α-Me)pTyr and β-bend-inducing motifs. As a further consideration, it was realized that, although several variants of (α-Me)pTyr that differ in the phosphoryl-mimicking 4-phenyl-substituted region have been examined in the pY + 1 position,[13,14] other modifications of (α-Me)pTyr, particularly those that introduce aspects of the Ac_6c residue, have not been reported. Therefore, studies were undertaken to address two issues. In the first study, structural components of Ac_6c and (α-Me)-Ppp were combined into a single residue represented by the tetralin-based (*S*)-2-amino-6-phosphonotetralin-2-carboxylic acid (Atc(6-PO_3H_2, depicted by **5**, Figure 1).[22] Atc(6-PO_3H_2) may be seen both as an (α-Me)Ppp residue that contains Ac_6c as a structural component (Figure 1) and as an (α-Me)Ppp variant that bears conformational constraint of side chain χ_1 and χ_2 angles.[22] For this study, open-chain peptides were prepared having Ac_6c, (α-Me)Ppp, and Atc(6-PO_3H_2) residues in the pY + 1 position (peptides **6**, **8**, and **9**, respectively). A second study was undertaken in which the Ac_6c residue in macrocycle **7** was replaced with an (α-Me)-Ppp residue to yield the corresponding globally constrained hybrid macrocycle **10**. Target peptides **9** and **10** from the aforementioned studies explore the application of local and global conformational constraint, respectively, to Grb2 SH2 domain binding peptides bearing pTyr mimetics in the pY + 1 position.

Synthesis

Coupling of asparagine 3-((1-naphthyl)propyl))amide (**11**)[23] with the sterically crowded *N*-Boc (α-Me)Phe(4-PO_3Et_2)-OH (**12**)[14,22] or with *N*-Boc (*S*)-2-amino-6-(diethylphosphono)tetralin-2-carboxylic acid (Boc-Atc(6-PO_3Et_2)-OH, **13**)[22] was accomplished using tetramethylfluoroformamidinium hexafluorophosphate (TFFH)[24] to yield dipeptides **14** and **15**, respectively (Scheme 1). After trifluoroacetic acid (TFA)-mediated *N*-Boc deprotection of both **14** and **15**, reaction with pTyr mimetic **16**[25] was conducted using TFFH activation to yield the globally protected products **17** and **18**, respectively. Final products **8** and **9** were obtained following a two-stage trimethylsilyliodide (TMSI) TFA deprotection protocol. The Ac_6c-containing peptide **6** has been reported previously.[25] Synthesis of (α-Me)Ppp-containing macrocycle **10** (Scheme 2) was similar to previously reported procedures.[18,20]

Results and Discussion

The objectives of the current work were to examine the Grb2 SH2 domain binding effects incurred by: (1) combining into a single analogue important structural features of (α-Me)Ppp and Ac_6c residues and (2) placing an (α-Me)pTyr mimetic at the pY + 1 position of a β-macrocyclized inhibitor. Objective 1 was accomplished using the tetralin-based Atc(6-PO_3H_2) (**5**) as a substitute for the pY + 1 Ac_6c residue in the known high-affinity (1-naphthyl)propylamide-containing pseudotripeptide **6**.

Scheme 1. Reagents and Conditions: (i) TFFH, *i*-Pr_2EtN and either **12** or **13**; (ii) (A) TFA, Anisole, (B) $NaHCO_3$, (C) **13**, TFFH, *i*-Pr_2EtN; (iii) (A) TMSI, (B) TFA/H_2O (95:5).

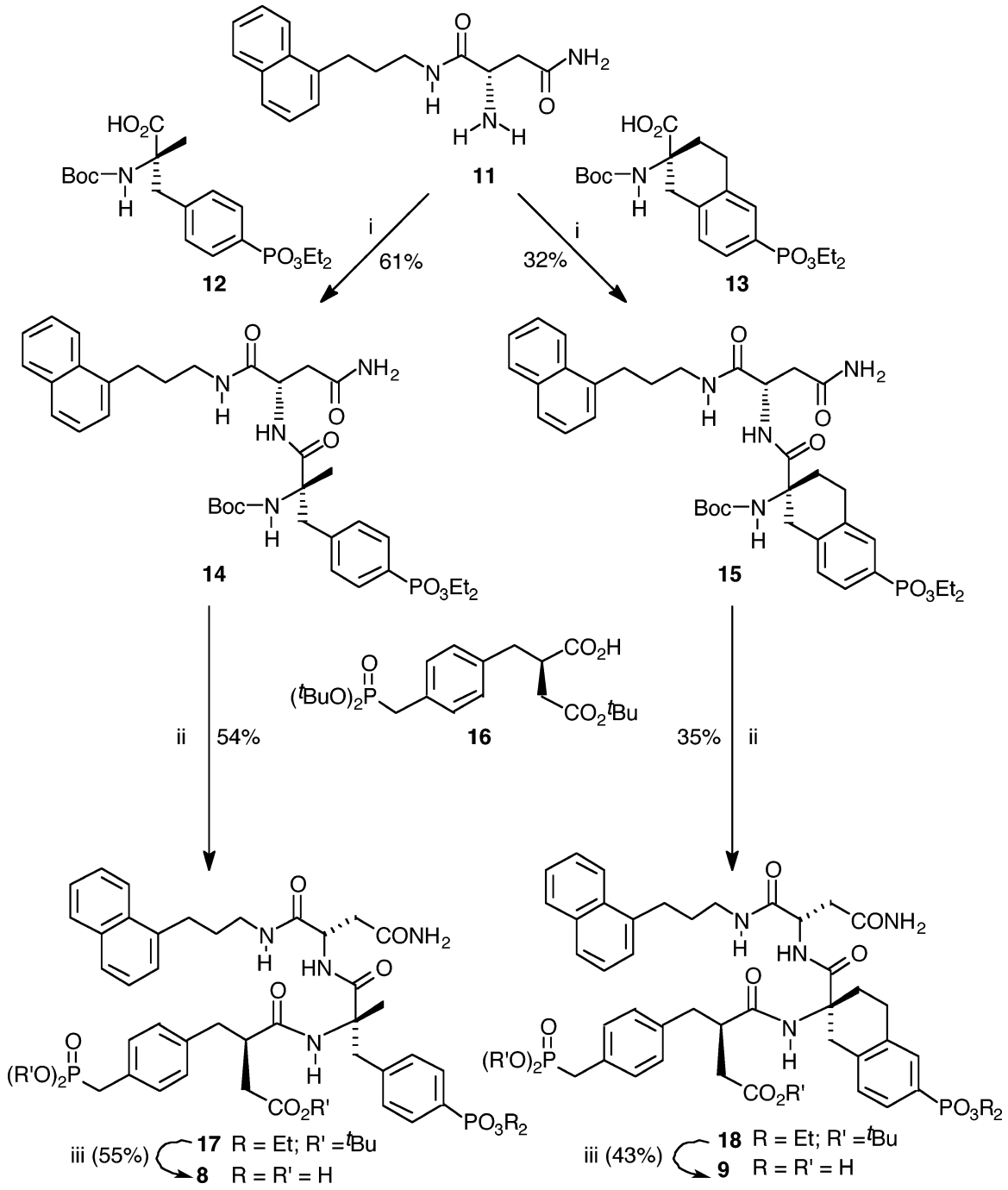

This latter peptide employs an α-carboxymethyl-containing pTyr mimetic in the pY^0 position.[25] Synthesis of the Atc(6-PO_3H_2)-containing title peptide **9** was achieved using the globally protected tetralin analogue **13**.[22] The binding potency of **9** was compared with the known Ac_6c-containing peptide **6**[25] and with the corresponding (α-Me)Ppp-containing peptide **8**. Evaluation of Grb2 SH2 domain binding potency was accomplished by plasmon resonance analysis using a Biacore instrument, which measured the direct binding of synthetic inhibitor to sensor-bound Grb2 SH2 domain protein.

Grb2 SH2 Domain Binding Affinities. Kinetic binding data in the form of on- and off-rates and associated K_D values for **6**, **8**, and **9** are shown in Table 1. The highest binding affinity of these three peptides was exhibited by the (α-Me)Ppp-containing **8** (K_D = 14.8 nM). The binding affinity of the Ac_6c-containing **6** (K_D = 23.8 nM)[26] was less than the affinity of **8**, although the difference between **6** and **8** was not as great as would be expected based on the 10-fold potency enhancement incurred by replacing the pY + 1 Ac_6c residue with an (α-Me)Ppp residue to yield peptide **26** (Figure 2).[14] It should be noted that peptides in the current study are based on the 3-(1-naphthyl)propanamido parent **6**, whereas analogues of the former study were based on a different peptide (Figure 2). Relative contributions to overall binding of the pY + 1 residue could be different for these two peptides. Interestingly, although the former study did report a prodrug-protected form of Ac-pY-(αMe)pY-N-[3-(1-naphthyl)-

Scheme 2. Reagents and Conditions: (i) **12**, TFFH, *i*-Pr_2EtN (38% yield); (ii) (A) TFA, Anisole, (B) $NaHCO_3$, (C) **21**, TFFH, *i*-Pr_2EtN (8% yield); (iii) **23**, CH_2Cl_2, Reflux (28% yield); (iv) (A) TMSI, (B) TFA/H_2O (95:5) (29% yield).

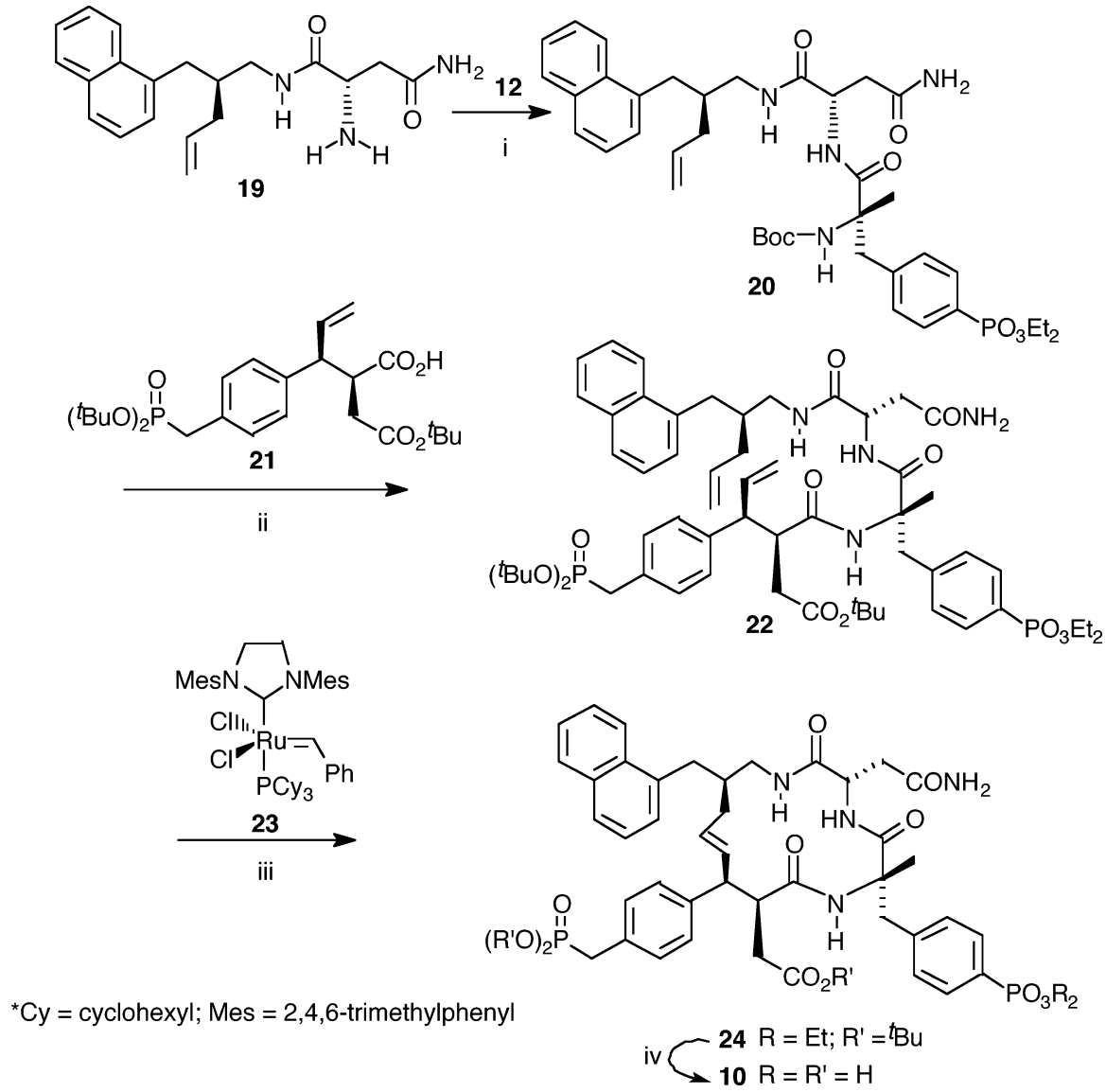

Table 1. In Vitro Grb2 SH2 Domain Binding Affinity[a]

no.	k_a (M^{-1} s^{-1})	k_d (s^{-1})	K_D (nM)
6	$4.18 \times 10^6 \pm 2.88 \times 10^5$	$9.91 \times 10^{-2} \pm 2.94 \times 10^{-3}$	23.8 ± 1.8
8	$4.50 \times 10^6 \pm 1.96 \times 10^4$	$6.65 \times 10^{-2} \pm 1.61 \times 10^{-4}$	14.8 ± 0.08
9	$6.09 \times 10^6 \pm 2.41 \times 10^5$	$5.94 \times 10^{-1} \pm 2.26 \times 10^{-3}$	97.8 ± 1.8
10	$2.03 \times 10^6 \pm 4.27 \times 10^3$	$4.63 \times 10^{-3} \pm 8.81 \times 10^{-6}$	2.28 ± 0.01

[a] Determined by plasmon resonance and evaluated by global analysis of at least four independent data sets as described in the Experimental Section.

propanamide], the binding affinity of the unprotected peptide was not provided.[14]

Examination of relative association and dissociation rates (k_a and k_d, respectively, Table 1) showed that the lower affinity of **6** was due primarily to a 50% increase in its rate of dissociation relative to **8**. Alternatively, combining features of the Ac_6c residue and the (α-Me)-Ppp residue into the Atc(6-PO_3H_2) residue in analogue **9** resulted in a net loss of inhibitory potency (K_D = 97.8 nM) despite a 35−45% enhancement in rate of association. The loss of binding affinity of **9** was attributed to a 6- to 9-fold increase in dissociation rate compared to **6** and **8**, respectively. Therefore, although combining key (α-Me)Ppp structural components into the Ac_6c residue did result in an increase in the rate of binding, this was accompanied by an unfavorable elevation in binding off-rate.

The second objective of the current study was to examine the effects of introducing global conformational constraint into open-chain **8** through conversion to the β-macrocycle **10**. An analysis of six independent experiments using a simple binding model provided a K_D value of 2.28 nM. The major contribution to affinity enhancement was provided by a more than 10-fold decrease in dissociation rate relative to open-chain **8**. However, it was noted that mathematical fitting using a simple model that assumed a single binding site did not closely approximate the data obtained, whereas use of a complex model that assumed two binding sites resulted in a very close fit of data. Figure 3 shows a single data set that has been fit according to simple (red) and complex (blue) models. It can be seen that the overall K_D value of 4.3 nM obtained from the simple model actually represents the combination of affinities derived from binding to two sites with K_D values of 97 pM and

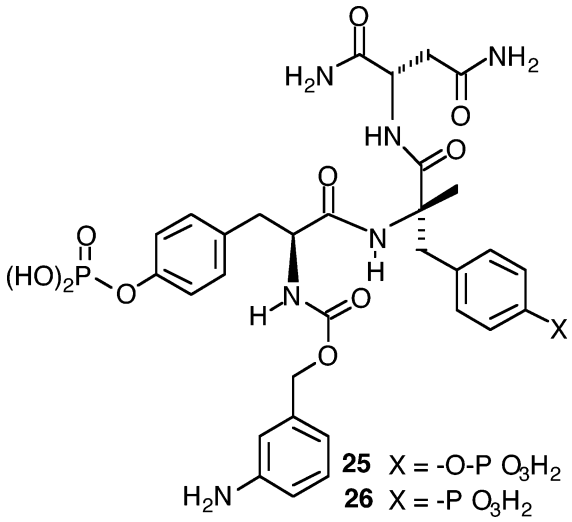

Figure 2. Structure of reference peptide **25**.

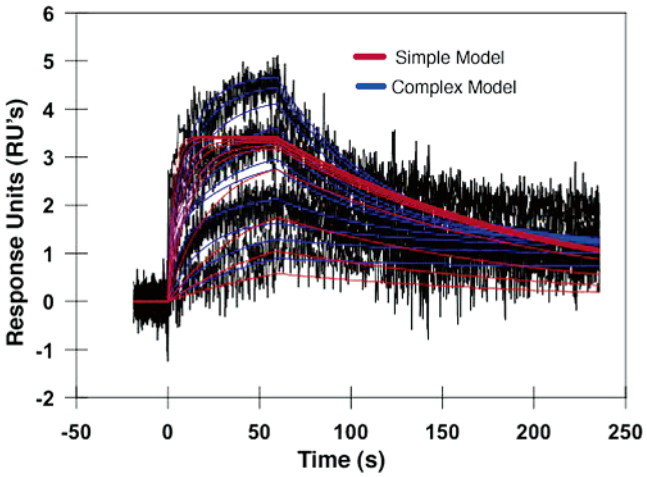

Figure 3. Plasmon resonance data derived from the binding of **10** to Grb2 SH2 domain protein showing mathematical fitting using either simple (red) or complex (blue) models.

Table 2. Kinetic Analysis of Binding Data Shown in Figure 3 Using Simple or Complex Binding Models[a]

no.	k_a (M^{-1} s^{-1})	k_d (s^{-1})	K_D (nM)
10	1.5×10^6	6.5×10^{-3}	4.3
10A	6.5×10^6	6.3×10^{-4}	0.097
10B	2.3×10^5	1.8×10^{-2}	72

[a] Determined by plasmon resonance. Analysis is of a single data set using either a simple binding model (for **10**) or a complex binding model (for **10A** and **10B**). Data used for these analyses are shown in Figure 3.

72 nM (Table 2). The mechanistic basis for this complex binding behavior is unclear, although it may indicate that in addition to the expected binding orientation shown in Figure 4D peptide **10** may be interacting with other sites or in nonstandard modes. Because this type of complex binding behavior was not observed with the flexible, open-chain peptides **6**–**9**, such secondary binding may be dependent on the macrocyclic nature of **10**.

Molecular Modeling. The interactions of peptides **6**, **8**, **9,** and **10** with the Grb2 SH2 domain protein were examined using molecular modeling techniques. The results of these calculations are shown graphically in Figure 4. Modeling of **9** was conducted in two separate studies. In one study, the plane of the cyclohexyl ring was parallel to that of the pY^0 phenyl ring in what will be referred to as an "equitorial" orientation ("conformation 1", Figure 4B). The second study placed the plane of the cyclohexyl ring perpendicular to that of the pY^0 phenyl ring in what will be referred to as an "axial" orientation ("conformation 2", Figure 4C). The interactions of the inhibitors with the Grb2 SH2 domain were measured using tools available within Insight II and are shown in Table 3. All compounds were found to make key hydrogen bonding (H-bonding) interactions with residues Arg67, Arg86, Ser90, His107, Lys109, and Leu120, with the carboxamide moiety of the pY + 2 Asn residue making two H-bonding interactions in a bidentate manner with the backbone carbonyl and NH of Lys109 as well as with the backbone carbonyl of Leu120. In addition, the backbone amide of the pY + 1 residue was H-bonded to the carbonyl of His107. The importance of these interactions for high-affinity binding is indicated by their presence in all reported crystal structures of ligated Grb2 SH2 domains. For compound **8**, the acidic phosphonate hydroxyls of the pY^0 residue make five H-bonding interactions: one each with the side chain hydroxyl groups of Ser88 and Ser90, one each with the guanidino group of Arg67 and Arg86, and one with the backbone amide of Ser90. The α-CH_2COOH group of **8** interacts with the side chain of Arg67 through two H-bonds. The pY + 1 phosphonate group of **8** makes two H-bonding interactions: one with the backbone amide of Arg142 and another with the side chain hydroxyl group of Ser141. In contrast, the macrocycle **10** has enhanced electrostatic interactions due to stronger interactions with the side chain hydroxyl of Ser90, the side chain guanidino group of Arg67, and the backbone amide and side chains of Arg142 and Asn143. The binding conformation of **10** is also stabilized by an intramolecular H-bond. Compound **9** has greater electrostatic interactions in conformation 1 than those seen in conformation 2, giving higher electrostatic interactions than those obtained with compound **8**. Binding of **9** in a conformation 1 orientation could potentially result in higher binding affinity than that exhibited by **8**. However, because conformation 1 is approximately 10 kcal/mol higher in energy than conformation 2, it would most likely not be the major conformer in solution. In addition to exhibiting weaker electrostatic interactions as compared to those of **8**, conformation 2 of **9** also has a lower van der Waals interaction energy. Consistent with experimentally observed binding data (Table 1), these results indicate that binding of **9** in a conformation 2 orientation would result in lower binding affinity than that for conformation 1 or that for compound **8**.

For Grb2 SH2 domain bound ligands containing an Ac_6c residue at the pY + 1 position, what we have referred to as an *axial* cyclohexyl ring conformation has been reported to predominate.[27] The higher binding affinity of the originally reported analogue **26** that contains a pY + 1 (α-Me)Ppp residue (Figure 2)[14] potentially may be attributable to a combination of favorable electrostatic and hydrophobic interactions. As can be seen from Table 3, the presence of the (1-naphthyl)propylamide moiety in compounds **6**, **8**, **9**, and **10** contributes substantially to more favorable van der Waals energies as compared to those of **25**. However, **25** exhibits more favorable electrostatic interactions than these former analogues. Enhancing electrostatic

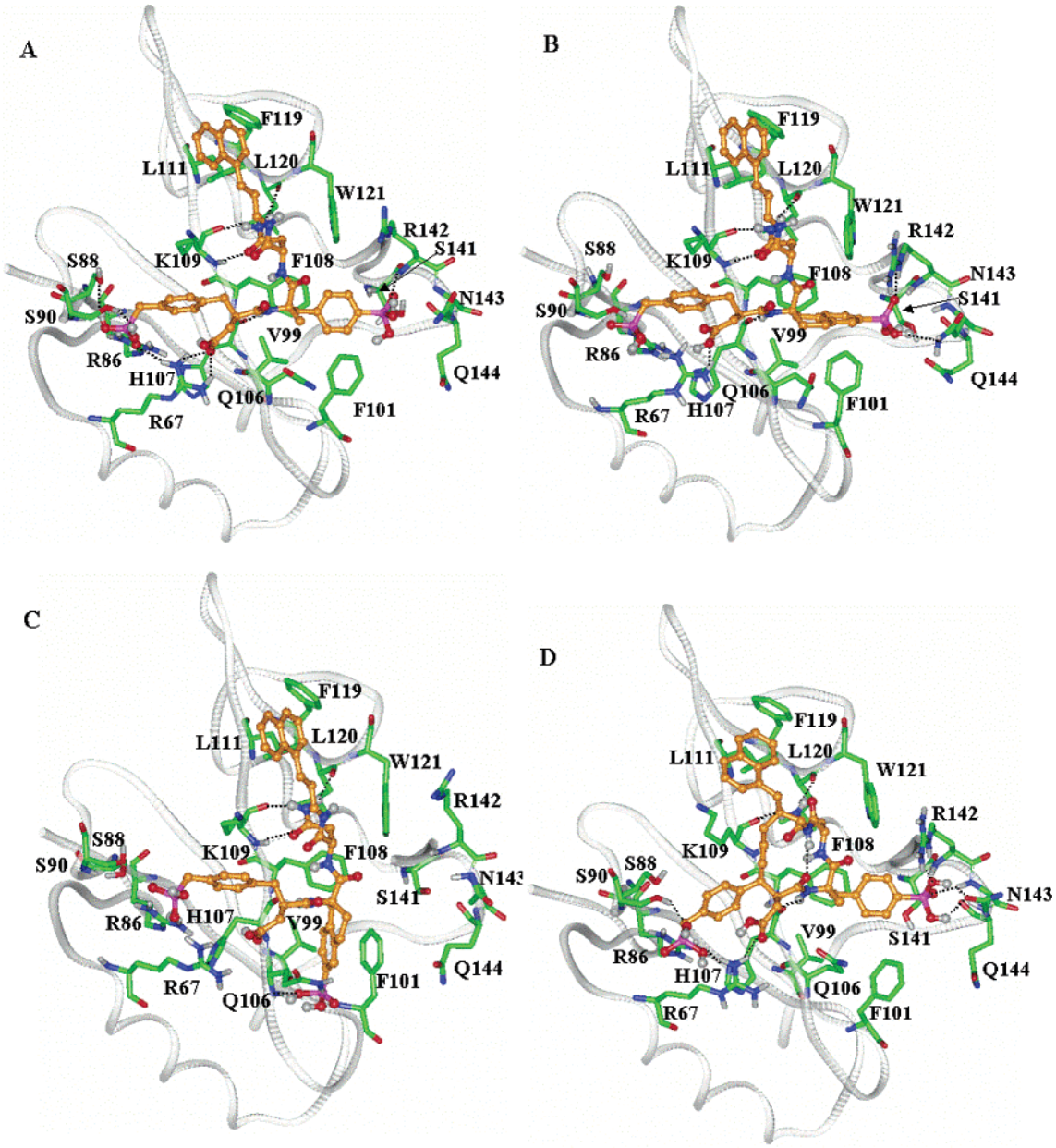

Figure 4. Hypothetical Grb2 SH2 domain binding modes of **8** (A), **9** with the pY + 1 cyclohexylphenyl ring in equatorial (B) and axial (C) orientations, and **10** (D). Hydrogen bonds are represented as dotted lines in black. For reasons of clarity, only key residues and atoms are shown.

Table 3. Calculated Energy Parameters Associated with Figure 4

parameter	compound **8** (A)[a] (kcal/mol)	compound **9** (B)[a] (kcal/mol)	compound **9** (C)[a] (kcal/mol)	compound **6** (kcal/mol)	compound **10** (D)[a] (kcal/mol)	compound **25** (kcal/mol)
van der Walls energy	−49.517	−45.905	−40.188	−39.897	−40.617	−38.355
coulomb energy	−50.942	−83.406	−19.479	−53.996	−93.296	−111.332

[a] The letter in parentheses refers to the panel in Figure 4 associated with the indicated parameters.

interactions in **8** and **9** could potentially result in higher binding affinity.

It should be noted that additional extensive modeling studies were performed, including conformational searches of the ligands using the Monte Carlo multiple minimum (MCMM) approach in Macromodel 8.0, flexible docking using GLIDE, and energy evaluations using ab initio methods in Gaussian 03. Although the results of these studies were not presented, they validated the results from the molecular dynamics simulations shown above and confirmed that the final positions of ligands within the binding site are the most stable conformations.

Conclusions

Structure−activity studies have previously identified the Ac_6c and (α-Me)Ppp residues as being among optimal pY + 1 residues for high Grb2 SH2 domain binding affinity. It was therefore of interest to investigate the binding effects of combining the structural features of these two residues into a single tetralin-

based analogue as shown by **5**, Figure 1. Indeed, replacement of the pY + 1 Ac_6c residue with this hybrid resulted in a 35−45% enhancement in binding on-rate. However, overall binding affinity was reduced due to a concomitant 6- to 9-fold increase in off-rates. Molecular modeling calculations indicated that electrostatic interactions may be major contributors to these binding effects. It can be concluded that local conformational constraint of the pY + 1 (α-Me)Ppp residue of peptide **8** failed to enhance overall binding affinity. Alternatively, global conformational constraint of the (α-Me)-Ppp-containing peptide **8** by *β*-macrocyclization to **10** did result in pronounced elevation of binding affinity, with the effect being achieved primarily through a decrease in the binding off-rate. Of note, mathematical fitting using a simple model that assumed a single binding site for **10** yielded an effective K_D of 2.28 nM. However, this did not closely approximate the data obtained. Rather, use of a complex model that assumed two binding sites resulted in a very close fit of data and provided K_D values of 97 pM and 72 nM for the separate sites, respectively. The value of global conformational constraint through *β*-macrocyclization may potentially be extended to SH2 domain systems other than Grb2 where bend geometries are required.

Experimental Section

Plasmon Resonance Analysis of Grb2 SH2 Domain Binding Affinity. Binding experiments were performed on a BIACORE S51 instrument (Biacore, Inc., Piscataway, NJ). All biotinylated Grb2 SH2 domain protein (b-Grb2) was expressed and purified (Protein Expression Laboratory and The Protein Chemistry Laboratory, SAIC−Frederick). The b-Grb2 was immobilized onto the carboxymethyl-5′-dextran surface (CM5 sensor chip, Biacore, Inc.) by amine coupling. The lyophilized b-Grb2 was reconstituted in 50% DMSO in H_2O to make a stock solution of 1 mg/mL and stored at −80° C. A 1:12.5 dilution of b-Grb2 was used for immobilization and prepared by dilution in acetate buffer pH 5.0, with 5% DMSO. Phosphate-buffered saline (PBS, 1×, pH 7.4) was used as the running buffer.

An immobilization wizard was used to facilitate immobilization targeting. For b-Grb2, 2500−5000 resonance units (RU) of protein were captured on the CM5 sensor chip. Small molecule ligands were serially diluted in running buffer to concentrations of 1.25−1500 nM, as described in each sensorgram, and injected at 25 °C at a flow rate of 30 *μ*L/min for 1 min, and dissociation was monitored for an additional 3 min. Surface regeneration was not used. Samples of differing concentrations of small molecule ligands were injected in increasing concentration, with every injection being performed in duplicate within each experiment. To subtract background noise from each data set, all samples were also run over an unmodified reference surface, and injections of running buffer were performed throughout every experiment ("double referencing"). Up to six data sets were fit to a simple 1:1 interaction model or to a surface heterogeneity model ("complex model") for compound **10**, using the global data analysis program CLAMP.[28] The mean of the ratio and associated error were calculated according to known procedures.[29]

Molecular Modeling. Simulations were performed with the Insight II 2000.0/Discover 97.0 modeling package (Molecular Simulations, Inc., San Diego, CA), using the cff91 force field.[30,31] The crystal structure of peptide **25** bound to Grb2 SH2 domain protein (PDB code 1JYQ[15]) was used as the starting geometry. The structure of **25** was first modified to yield inhibitors **8**, **9**, and **10**. In the case of **9**, the conformation of the pY + 1 cyclohexyl ring was modeled separately in equitorial (the plane of the cyclohexyl ring being parallel to that of the pY^0 phenyl ring) and axial (the plane of the cyclohexyl ring perpendicular to that of the pY^0 phenyl ring) orientations (conformation 1 and conformation 2, respectively). The resulting protein−ligand structures were solvated with a 30 Å sphere of H_2O (3160 molecules) and subjected to 1000 steps of energy minimization with the steepest descent method followed by 500 steps of the Polak−Ribiere conjugate-gradient algorithm (CG-PR). The minimized complex was subjected to 50 ps of an NVT molecular dynamics (MD) simulation at 298 K. The coordinates were saved every 100 fs and subsequently minimized by 500 steps of CG-PR. During minimization and simulation, all atoms were held fixed except for those within a 10 Å sphere around the inhibitors, including H_2O molecules. For each inhibitor, the frame with the lowest energy among the 500 minimized frames is depicted in Figure 4. For purposes of comparison, peptide **25** was also subjected to minimization and MD simulation as described above. The intermolecular interaction energies between the bound inhibitor and the protein in the lowest energy frame were evaluated using tools available within Insight II[30] and are shown in Table 3.

General Synthetic. Reactions were carried out under argon. Anhydrous solvents were purchased from Aldrich Chemical Corporation and used without further drying. Combustion analyses were obtained from Atlantic Microlab, Inc., Norcross, GA. ^{1}H NMR spectra were obtained using a Varian 400 MHz spectrometer and are reported in ppm relative to TMS and referenced to the solvent in which they were run. Fast atom bombardment mass spectra (FABMS) were acquired with a VG analytical 7070E mass spectrometer. HPLC separations were conducted using a Waters Prep LC4000 system with photodiode array detection and a J-sphere ODS-H80 column (20 mm × 250 mm) with a solvent system consisting of 0.1% aqueous TFA (v/v, solvent A)/0.1% TFA in MeCN (v/v, solvent B).

Boc-(α-Me)Phe(4-PO_3Et_2)-Asn-$(CH_2)_3$-(1-naphthyl) (14). To a stirred solution of (*S*)-asparagine 3-(1-naphthyl)propylamide (**11**)[23] (200 mg, 0.668 mmol) in dry DMF (2 mL) were added Boc-(α-Me)Phe(4-PO_3Et_2)-OH (**12**)[14,22] (305 mg, 0.734 mmol), tetramethylfluoroformamidinium hexafluorophosphate (TFFH)[24] (194 mg, 0.734 mmol), and *i*-Pr_2NEt (0.254 mL, 1.46 mmol) at 0 °C, and stirring was continued for 24 h at room temperature. The mixture was extracted with EtOAc, and the extract was washed successively with saturated citric acid solution, brine, saturated $NaHCO_3$ solution, and brine and dried over Na_2SO_4. Concentration followed by flash chromatography over silica gel using CH_2Cl_2/MeOH (100:0 to 10:1) provided **14** as colorless semisolid (287 mg, 61% yield). ^{1}H NMR ($CDCl_3$): *δ* 1.33 (m, 6 H), 1.37 (s, 9 H), 1.48 (s, 2 H), 1.98 (m, 2 H), 2.23 (dd, *J* = 15.6 and 5.1 Hz, 1 H), 2.98 (d, *J* = 13.6 Hz, 1 H), 3.02 (dd, *J* = 15.6 and 3.9 Hz, 1 H), 3.09 (t, *J* = 7.5 Hz, 2 H), 3.28 (m, 1 H), 3.30 (d, *J* = 13.1 Hz, 1 H), 3.38 (m, 1 H), 4.12 (m, 4 H), 4.62 (m, 1 H), 4.86 (s, 1 H), 5.32 (br, 1 H), 6.05 (br, 1 H), 7.24 (dd, *J* = 8.2 and 3.9 Hz, 2 H), 7.30−7.56 (m, 5 H), 7.68 (d, *J* = 8.5 Hz, 1 H), 7.74 (dd, *J* = 13.1 and 8.2 Hz, 2 H), 7.81 (m, 2 H), 8.02 (d, *J* = 7.3 Hz, 1 H). FABMS *m/z*: 697 (MH^+). Anal. Calcd for $C_{36}H_{49}N_4O_8P\cdot 0.8H_2O$: C, 60.80; H, 7.17; N, 7.88. Found: C, 60.92; H, 7.12; N, 7.92.

Boc-Atc(6-PO_3Et_2)-Asn-$(CH_2)_3$-(1-naphthyl) (15). Coupling of **11** (200 mg, 0.668 mmol) with Boc-(*S*)-2-amino-6-(diethylphosphono)tetralin-2-carboxylic acid (Boc-Atc(6-PO_3Et_2)-OH) **13**[22] in a manner similar to that described above for the preparation of **14**, provided **15** as a colorless semisolid (154 mg, 32% yield). ^{1}H NMR ($CDCl_3$): *δ* 1.34 (m, 15 H), 2.00 (m, 2 H), 2.31 (m, 1 H), 2.48 (dd, *J* = 15.3 and 4.8 Hz, 1 H), 2.58 (m, 1 H), 2.72 (m, 1 H), 2.85 (d, *J* = 17.0 Hz, 1 H), 2.92 (m, 1 H), 3.13 (m, 3 H), 3.25 (m, 1 H), 3.32 (d, *J* = 16.8 Hz, 1 H), 3.44 (m, 1 H), 4.12 (m, 4 H), 4.78 (m, 1 H), 4.92 (s, 1 H), 5.33 (br, 1 H), 6.10 (br, 1 H), 7.14 (dd, *J* = 7.8 and 4.1 Hz, 1 H), 7.32−7.74 (m, 8 H), 7.83 (d, *J* = 7.8 Hz, 1 H), 8.05 (d, *J* = 8.0 Hz, 1 H), 8.31 (d, *J* = 8.2 Hz, 1 H). FABMS *m/z*: 709 (MH^+). Anal. Calcd for $C_{37}H_{49}N_4O_8P\cdot 0.5H_2O$: C, 61.91; H, 7.02; N, 7.81. Found: C, 61.92; H, 7.02; N, 7.81.

[(2*R*)-2-(*tert*-Butyloxycarbonylmethyl)-3-(4-di-*tert*-butylphosphonomethyl)phenylpropionyl]-(α-Me)Phe-

(4-PO_3Et_2)-Asn-$(CH_2)_3$-(1-naphthyl) (17). Protected peptide **14** (316 mg, 0.453 mmol) was treated with TFA/anisole (10:1, 5.5 mL) for 2 h at room temperature. The mixture was concentrated and neutralized with saturated $NaHCO_3$ solution. The mixture was extracted with EtOAc, and the extract was washed with saturated $NaHCO_3$ solution and brine and dried over Na_2SO_4. Concentration under reduced pressure gave the corresponding amine. To a stirred solution of the amine in dry DMF (1.4 mL) were added protected pTyr mimetic **16**[25] (307 mg, 0.498 mmol), TFFH (131 mg, 0.498 mmol), and *i*-Pr_2NEt (0.173 mL, 0.997 mmol) at 0 °C, and stirring was continued for 2 days at room temperature. The mixture was extracted with EtOAc, and the extract was washed successively with 5% citric acid solution, brine, saturated $NaHCO_3$ solution, and brine, and dried over Na_2SO_4. Concentration followed by flash chromatography over silica gel using CH_2Cl_2/MeOH (100:0 to 10:1) provided **17** as a colorless semisolid (260 mg, 54% yield). ^{1}H NMR (400 MHz, $CDCl_3$): δ 1.31 (m, 6 H), 1.36 (s, 9 H), 1.40 (s, 9 H), 1.41 (s, 9 H), 1.44 (s, 3 H), 2.04 (m, 2 H), 2.21 (dd, J = 17.7 and 3.3 Hz, 1 H), 2.47 (m, 3 H), 2.77 (m, 1 H), 2.84−3.04 (m, 5 H), 3.14 (m, 2 H), 3.24 (d, J = 13.6 Hz, 1 H), 3.37 (m, 2 H), 3.73 (m, 4 H), 4.55 (m, 1 H), 5.33 (br, 1 H), 6.29 (br, 1 H), 6.48 (s, 1 H), 6.98 (d, J = 7.9 Hz, 2 H), 7.17 (m, 4 H), 7.32−7.58 (m, 6 H), 7.69 (m, 3 H), 7.82 (d, J = 7.6 Hz, 1 H), 8.07 (d, J = 8.1 Hz, 1 H). FABMS *m/z*: 1049 (MH^+). Anal. Calcd for $C_{55}H_{78}N_4O_{12}P_2 \cdot H_2O$: C, 61.90; H, 7.56; N, 5.25. Found: C, 61.85; H, 7.55; N, 5.32.

[(2*R*)-2-(*tert*-Butyloxycarbonylmethyl)-3-(4-di-*tert*-butylphosphonomethyl)phenylpropionyl]-Atc(6-PO_3Et_2)-Asn-$(CH_2)_3$-(1-naphthyl) (18). Coupling of **15** (120 mg, 0.169 mmol) with **16** by a procedure similar to that described above for the preparation of the protected peptide **17** from **14**, provided **18** as a colorless semisolid (64 mg, 35% yield). ^{1}H NMR ($CDCl_3$): δ 1.31 (m, 6 H), 1.33 (s, 9 H), 1.38 (s, 9 H), 1.39 (s, 9 H). 1.94−2.11 (m, 2 H), 2.14 (dd, J = 17.5 and 3.4 Hz, 1 H), 2.25 (m, 1 H), 2.46 (m, 3 H), 2.64 (dd, J = 15.1 and 5.1 Hz, 1 H), 2.74 (m, 1 H), 2.78−2.91 (m, 4 H), 2.92−3.04 (m, 3 H), 3.13 (m, 2 H), 3.38 (m, 3 H), 4.09 (m, 4 H), 4.71 (m, 1 H), 5.32 (br, 1 H), 6.19 (br, 1 H), 6.27 (s, 1 H), 6.89 (d, J = 8.0 Hz, 2 H), 7.11 (m, 3 H), 7.38 (m, 2 H), 7.42−7.60 (m, 5 H), 7.70 (dd, J = 6.8 and 2.9 Hz, 1 H), 7.79 (d, J = 8.2 Hz, 1 H), 7.84 (d, J = 8.0 Hz, 1 H), 8.09 (d, J = 7.3 Hz, 1 H). FABMS *m/z*: 1061 (MH^+). Anal. Calcd for $C_{56}H_{78}N_4O_{12}P_2 \cdot H_2O$: C, 62.32; H, 7.47; N, 5.19. Found: C, 62.00; H, 7.44; N, 5.55.

[(2*R*)-3-(4-Phosphonomethyl)phenyl-2-(carboxymethyl)propionyl]-(α-Me)Phe(4-PO_3H_2)-Asn-$(CH_2)_3$-(1-naphthyl) (8). To a stirred solution of protected peptide **17** (30 mg, 0.0285 mmol) in MeCN (1 mL) were added thioanisole (0.100 mL) and trimethylsilyliodide (TMSI) (0.711 mL) at 0 °C. The mixture was stirred for 30 min at 0 °C and an additional 1 h at room temperature. After concentration, the residue was dissolved in 95% TFA solution (10 mL), and stirring was continued for 2 h at room temperature. The mixture was concentrated and extracted with H_2O, and the extract was washed with Et_2O. The aqueous solution was purified by preparative HPLC using a linear gradient 30% to 35% B over 20 min to provide **8** as a colorless powder (13 mg, 55% yield). ^{1}H NMR (DMSO-d_6): δ 1.17 (s, 3 H), 1.87 (m, 2 H), 2.01 (dd, J = 16.9 and 4.8 Hz, 1 H), 2.41 (dd, J = 15.2 and 10.7 Hz, 1 H), 2.47−2.73 (m, 4 H), 2.86−3.31 (m, 9 H), 4.28 (m, 1 H), 6.89 (s, 1 H), 7.03 (m, 4 H), 7.16 (m, 2 H), 7.34 (s, 1 H), 7.38−7.45 (m, 6 H), 7.58 (t, J = 5.3 Hz, 1 H), 7.76 (dd, J = 6.8 and 2.1 Hz, 1 H), 7.85 (d, J = 7.8 Hz, 1 H), 7.90 (m, 1 H), 8.13 (d, J = 7.8 Hz, 1 H), 8.48 (s, 1 H). FABMS *m/z*: 823 [$(M - H)^-$].

[(2*R*)-3-(4-Phosphonomethyl)phenyl-2-(carboxymethyl)propionyl]-Atc(6-PO_3H_2)-Asn-$(CH_2)_3$-(1-naphthyl) (9). Treatment of **18** (32 mg, 0.0301 mmol) as described above for the preparation of **8** provided **9** as colorless powder (11 mg, 43% yield). ^{1}H NMR (DMSO-d_6): δ 1.78−2.06 (m, 4 H), 2.18 (m, 1 H), 2.32−2.54 (m, 3 H), 2.66 (m, 1 H), 2.75−3.30 (m, 12 H), 4.42 (m, 1 H), 6.82 (d, J = 7.8 Hz, 2 H), 6.95 (s, 1 H), 7.02 (m, 2 H), 7.15 (dd, J = 7.8 and 3.6 Hz, 1 H), 7.35−7.57 (m, 8 H), 7.78 (dd, J = 5.8 and 3.6 Hz, 1 H), 7.92 (m, 1 H), 8.08 (d, J = 8.3 Hz, 1 H), 8.15 (d, J = 8.0 Hz, 1 H), 8.71 (s, 1 H). FABMS *m/z*: 835 [$(M - H)^-$].

(2*S*)-3-(4-Bisethoxyphosphono)phenyl-2-(*tert*-butoxycarbonyl)amino-2-methyl-*N*-((1*S*)-1-{*N*-[(2*S*)-2-(naphthylmethyl)pent-4-enyl]carbamoyl}-2-carbamoylethyl)propylamide (20). Coupling of (2*S*)-2-amino-N^1-[(2*S*)-2-(1-naphthalenylmethyl)-4-pentenyl]butanediamide (**19**)[17] (300 mg, 0.883 mmol) with Boc-(α-Me)Phe(4-PO_3Et_2)-OH (**7**) **12** in a manner similar to that described above for the preparation of **14** provided **20** as a colorless semisolid (258 mg, 38% yield). ^{1}H NMR (400 MHz, $CDCl_3$): δ 1.29 (s, 9 H), 1.33 (m, 6 H), 1.45 (s, 3 H), 2.04−2.20 (m, 3 H), 2.23 (dd, J = 1.5 and 5.3 Hz, 1 H), 2.95−3.10 (m, 5 H), 3.29 (d, J = 13.4 Hz, 1 H), 3.44 (m, 1 H), 4.13 (m, 4 H), 4.62 (m, 1 H), 4.82 (s, 1 H), 5.02−5.13 (m, 2 H), 5.34 (br, 1 H), 5.83 (m, 1 H), 6.02 (br, 1 H), 7.23 (m, 2 H), 7.29−7.53 (m, 5 H), 7.66−7.84 (m, 5 H), 8.00 (d, J = 8.5 Hz, 1 H). FABMS *m/z*: 737 (MH^+).

***N*-{(1*S*)-2-(4-Bisethoxyphosphono)phenyl-1-methyl-1-[*N*-((1*S*)-1-{*N*-[(2*S*)-2-(naphthylmethyl)pent-4-enyl]-carbamoyl}-2-carbamoylethyl)carbamoyl]ethyl}-(2*S*,3*R*)-2-(*tert*-butoxycarbonylmethyl)-3-{4-[bis(*tert*-butoxy)-phosphonomethyl]phenyl}pente-4-enamide (22).** Coupling of (2*S*,3*S*)-3-(4-{[bis(*tert*-butoxy)phosphono]methyl}-phenyl)-2-{[(*tert*-butyl)oxycarbonyl]methyl}pent-4-enoic acid (**21**)[18] (120 mg, 0.169 mmol) with **20** by a procedure similar to that described above for the preparation of the protected peptide **17** from **14** provided **22** as a colorless semisolid (30 mg, 8% yield). ^{1}H NMR (400 MHz, $CDCl_3$): δ 1.19 (s, 3 H), 1.32 (t, J = 7.0 Hz, 6 H), 1.40 (s, 9 H), 1.41 (s, 9 H), 1.42 (s, 9 H), 2.02−2.24 (m, 3 H), 2.39 (dd, J = 18.0 and 9.7 Hz, 1 H), 2.54 (m. 3 H), 2.82−3.19 (m, 8 H), 3.24 (m, 1 H), 3.41 (m, 1 H), 4.11 (m, 4 H), 4.64 (m, 1 H), 4.93 (m, 2 H), 5.10 (m, 2 H), 5.64 (m, 1 H), 5.87 (m, 1 H), 6.43 (s, 1 H), 6.64 (d, J = 7.8 Hz, 1 H), 6.80−7.20 (m, 7 H), 7.32−7.56 (m, 5 H), 7.67 (m, 3 H), 7.83 (d, J = 7.8 Hz, 1 H), 8.06 (d, J = 8.3 Hz, 1 H). FABMS *m/z*: 1115 (MH^+).

2-[(1*S*,5*S*,9*R*,13*S*)-3,12,15-Triaza-13-(4-Bisethoxyphosphono)phenylmethyl-9-[4-bis(*tert*-butoxy)phosphono-methyl]phenyl-13-methyl-5-naphthylmethyl-2,11,14-trioxocyclopentadec-7-enyl]acetamide (24). To a solution of **22** (25 mg, 0.022 mmol) in CH_2Cl_2 (5.5 mL) was added ruthenium catalyst **23** (9.5 mg, 0.011 mmol) in CH_2Cl_2 (1.8 mL) under argon. The reaction was stirred at 45 °C for 24 h. The crude reaction mixture was evaporated in vacuo, and the residue was purified by silica gel chromatography using CH_2Cl_2/MeOH (10:1) to provide **24** as a colorless powder (7 mg, 28% yield). ^{1}H NMR (400 MHz, $CDCl_3$): δ 1.18−1.46 (m, 33 H), 1.59 (s, 3 H), 1.78−1.91 (m, 2 H), 2.14 (m, 2 H), 2.30 (m, 1 H), 2.63 (dd, J = 13.2 and 10.0 Hz, 1 H), 2.68−3.13 (m, 8 H), 3.34 (dd, J = 13.7 and 4.6 Hz, 1 H), 3.75 (dd, J = 13.0 and 5.6 Hz, 1 H), 3.86 (m, 1 H), 4.11 (m, 4 H), 4.55 (m, 1 H), 4.98 (br, 1 H), 5.36 (ddd, J = 14.8, 10.2 and 2.8 Hz, 1 H), 5.74 (dd, J = 14.8 and 11.8 Hz, 1 H), 5.84 (br, 1 H), 6.32 (s, 1 H), 7.05−7.52 (m, 12 H), 7.64−7.82 (m, 4 H), 8.16 (d, J = 8.6 Hz, 1 H). FABMS *m/z*: 1087 (MH^+).

2-[(1*S*,5*S*,9*R*,13*S*)-3,12,15-Triaza-13-(4-phosphono)-phenylmethyl-9-(4-phosphonomethyl)phenyl-13-methyl-5-naphthylmethyl-2,11,14-trioxocyclopentadec-7-enyl]-acetamide (10). Treatment of **24** (6.5 mg, 0.0301 mmol) as described above for the preparation of **8** provided **10** as colorless powder (1.5 mg, 29% yield). ^{1}H NMR (400 MHz, DMSO-d_6): δ 1.90−2.22 (m, 8 H), 2.39 (m, 1 H), 2.60 (m, 1 H), 2.64−2.88 (m, 6 H), 3.08 (d, J = 12.8 Hz, 1 H), 3.14−3.26 (m, 2 H), 3.57 (m, 1 H), 4.01 (m, 1 H), 4.26 (m, 1 H), 5.46 (m, 1 H), 5.81 (m, 1 H), 7.02 (s, 1 H), 7.16−7.29 (m, 6 H), 7.37−7.59 (m, 8 H), 7.76 (m, 1 H), 7.90 (d, J = 8.1 Hz, 1 H), 8.17 (d, J = 8.6 Hz, 1 H), 8.29 (d, J = 8.2 Hz, 1 H), 8.89 (s, 1 H). LRMS (FAB) *m/z*: 861 [$(M-H)^-$].

Acknowledgment. Appreciation is expressed to Drs. James Kelley and Christopher Lai of the LMC for mass spectral analysis and to Dr. Megan Peach for helpful molecular modeling discussions. Support was provided by the Japan Society for the Promotion of

Science in the form of a Postdoctoral Fellowship for Research Abroad (to S.O.).

References

(1) Daly, R. J.; Binder, M. D.; Sutherland, R. L. Overexpression of the Grb2 gene in human breast cancer cell lines. *Oncogene* **1994**, *9*, 2723−2727.

(2) Sastry, L.; Cao, T.; King, C. R. Multiple Grb2-protein complexes in human cancer cells. *Int. J. Cancer* **1997**, *70*, 208−213.

(3) Million, R. P.; VanEtten, R. A. The Grb2 binding site is required for the induction of chronic myeloid leukemia-like disease in mice by the Bcr/Abl tyrosine kinase. *Blood* **2000**, *96*, 664−670.

(4) Tari, A. M.; Lopez-Berestein, G. GRB2: A pivotal protein in signal transduction. *Semin. Oncol.* **2001**, *28*, 142−147.

(5) Dankort, D.; Maslikowski, B.; Warner, N.; Kanno, N.; Kim, H.; Wang, Z. X.; Moran, M. F.; Oshima, R. G.; Cardiff, R. D.; Muller, W. J. Grb2 and Shc adapter proteins play distinct roles in Neu (ErbB-2)-induced mammary tumorigenesis: Implications for human breast cancer. *Mol. Cell. Biol.* **2001**, *21*, 1540−1551.

(6) Saucier, C.; Papavasiliou, V.; Palazzo, A.; Naujokas, M. A.; Kremer, R.; Park, M. Use of signal specific receptor tyrosine kinase oncoproteins reveals that pathways downstream from Grb2 or Shc are sufficient for cell transformation and metastasis. *Oncogene* **2002**, *21*, 1800−1811.

(7) Vu, C. B. Recent advances in the design and synthesis of SH2 inhibitors of Src Grb2 and ZAP-70. *Curr. Med. Chem.* **2000**, *7*, 1081−1100.

(8) Fretz, H.; Furet, P.; Garcia-Echeverria, C.; Rahuel, J.; Schoepfer, J. Structure-based design of compounds inhibiting Grb2-SH2 mediated protein−protein interactions in signal transduction pathways. *Curr. Pharm. Des.* **2000**, *6*, 1777−1796.

(9) Garcia-Echeverria, C. Antagonists of the Src homology 2 (SH2) domains of Grb2, Src, Lck and ZAP-70. *Curr. Med. Chem.* **2001**, *8*, 1589−1604.

(10) Residue numbering is sequential in the C-terminal direction.

(11) Furet, P.; Gay, B.; Caravatti, G.; GarciaEcheverria, C.; Rahuel, J.; Schoepfer, J.; Fretz, H. Structure-based design and synthesis of high affinity tripeptide ligands of the Grb2-SH2 domain. *J. Med. Chem.* **1998**, *41*, 3442−3449.

(12) Nomenclature is as proposed by Eck et al. in *Nature* **1993**, *362*, 87−91.

(13) Liu, W. Q.; Vidal, M.; Gresh, N.; Rogues, B. P.; Garbay, C. Small peptides containing phosphotyrosine and adjacent alpha Me-phosphotyrosine or its mimetics as highly potent inhibitors of Grb2 SH2 domain. *J. Med. Chem.* **1999**, *42*, 3737−3741.

(14) Liu, W.-Q.; Vidal, M.; Olszowy, C.; Million, E.; Lenoir, C.; Dhotel, H.; Garbay, C. Structure−activity relationships of small phosphopeptides, inhibitors of Grb2 SH2 domain, and their prodrugs. *J. Med. Chem.* **2004**, *47*, 1223−1233.

(15) Nioche, P.; Liu, W.-Q.; Broutin, I.; Charbonnier, F.; Latreille, M.-T.; Vidal, M.; Roques, B.; Garbay, C.; Ducruix, A. Crystal structures of the SH2 Domain of Grb2: Highlight on the binding of a new high-affinity inhibitor. *J. Mol. Biol.* **2002**, *315*, 1167−1177.

(16) Gao, Y.; Voigt, J.; Wu, J. X.; Yang, D.; Burke, T. R., Jr. Macrocyclization in the design of a conformationally constrained Grb2 SH2 domain inhibitor. *Bioorg. Med. Chem. Lett.* **2001**, *11*, 1889−1892.

(17) Gao, Y.; Wei, C.-Q.; Burke, T. R., Jr. Olefin metathesis in the design and synthesis of a globally constrained Grb2 SH2 domain inhibitor. *Org. Lett.* **2001**, *3*, 1617−1620.

(18) Wei, C.-Q.; Gao, Y.; Lee, K.; Guo, R.; Li, B.; Zhang, M.; Yang, D.; Burke, T. R., Jr. Macrocyclization in the design of Grb2 SH2 domain-binding ligands exhibiting high potency in whole cell systems. *J. Med. Chem.* **2003**, *46*, 244−254.

(19) Shi, Z.-D.; Lee, K.; Liu, H.; Zhang, M.; Roberts, L. R.; Worthy, K. M.; Fivash, M. J.; Fisher, R. J.; Yang, D.; Burke, T. R. A novel macrocyclic tetrapeptide mimetic that exhibits low-picomolar Grb2 SH2 domain-binding affinity. *Biochem. Biophys. Res. Commun.* **2003**, *310*, 378−383.

(20) Shi, Z.-D.; Wei, C.-Q.; Lee, K.; Liu, H.; Zhang, M.; Araki, T.; Roberts, L. R.; Worthy, K. M.; Fisher, R. J.; Neel, B. G.; Kelley, J. A.; Yang, D.; Burke, T. R., Jr. Macrocyclization in the Design of Non-Phosphorus-Containing Grb2 SH2 Domain-Binding Ligands. *J. Med. Chem.* **2004**, *47*, 2166−2169.

(21) Shi, Z.-D.; Lee, K.; Wei, C.-Q.; Roberts, L. R.; Worthy, K. M.; Fisher, R. J.; Burke, T. R., Jr. Synthesis of a 5-methylindolyl-containing macrocycle that displays ultrapotent Grb2 SH2 domain-binding affinity. *J. Med. Chem.* **2004**, *47*, 788−791.

(22) Oishi, S.; Kang, S.-U.; Liu, H.; Zhang, M.; Yang, D.; Deschamps, J. R.; Burke, T. R. Synthesis of α,α-disubstituted 4-phosphonophenylalanine analogues as conformationally constrained phosphotyrosyl mimetics. *Tetrahedron* **2004**, *60*, 2971−2977.

(23) Yao, Z. J.; King, C. R.; Cao, T.; Kelley, J.; Milne, G. W. A.; Voigt, J. H.; Burke, T. R. Potent inhibition of Grb2 SH2 domain binding by nonphosphate-containing ligands. *J. Med. Chem.* **1999**, *42*, 25−35.

(24) Carpino, L. A.; El-Faham, A. Tetramethylfluoroformamidinium Hexafluorophosphate: A Rapid-Acting Peptide Coupling Reagent for Solution and Solid-Phase Peptide Synthesis. *J. Am. Chem. Soc.* **1995**, *117*, 5401−5402.

(25) Wei, C.-Q.; Li, B.; Guo, R.; Yang, D.; Burke, T. R., Jr. Development of a phosphatase-stable phosphotyrosyl mimetic suitably protected for the synthesis of high affinity Grb2 SH2 domain-binding ligands. *Bioorg. Med. Chem. Lett.* **2002**, *12*, 2781−2784.

(26) Through use of a noinetic ELISA-based Grb2 SH2 domain binding assay, the affinity of compound **6** has previously been reported in ref 25 as $IC_{50} = 8$ nM.

(27) Furet, P.; Garcia-Echeverria, C.; Gay, B.; Schoepfer, J.; Zeller, M.; Rahuel, J. Structure-based design, synthesis, and X-ray crystallography of a high-affinity antagonist of the Grb2-SH2 domain containing an asparagine mimetic. *J. Med. Chem.* **1999**, *42*, 2358−2363.

(28) Myszka, D. G.; Morton, T. A. CLAMP: A biosensor kinetic data analysis program. *Trends Biochem. Sci.* **1998**, *23*, 149−150.

(29) van Kempen, G. M.; van Vliet, L. J. Mean and variance of ratio estimators used in fluorescence ratio imaging. *Cytometry* **2000**, *39*, 300−305.

(30) Computational results were obtained using Insight II by Accelrys, Inc., San Diego, CA, 2000 (http://www.accelrys.com).

(31) Maple, J. R.; Dinur, U.; Hagler, A. T. Derivation of force fields for molecular mechanics and dynamics from ab initio energy surfaces. *Proc. Natl. Acad. Sci. U.S.A.* **1988**, *85*, 5350−5354.

(32) Available from Bachem. Corp., catalogue number B-2825.

JM0492709